Critical linkages of coalescing microcracks under stress loading

T. LI and W. YANG
Department of Engineering Mechanics, Tsinghua University, Beijing, 100084, P. R. China

Received in final form 20 September 2001

ABSTRACT The fracture process of brittle materials with randomly orientated microcracks critically depends on strong interactions among microcracks and the coalescence path that leads to a fatal crack. In this paper, a model based on the coalescence process for planar orientated microcracks is presented. An energy ratio is defined as the competition between the potential energy release and the new crack surface energy in each coalescence step, which is a token of the excessive driving force for microcrack propagation. A critical linkage dictates the coalescence of microcracks under stress loading. Probabilities of microcrack coalescence dominated by the first linkage and subsequent linkages are analysed for collinear and wavy microcrack arrays in detail.

Keywords coalescence; critical linkage; energy ratio; microcracks; probability; stress loading.

NOMENCLATURE

a_0 = expected half-length of distributed microcracks
a_1, a_2 = half-length of microcracks 1 and 2
c = ligament size
s_c = standard deviation of ligament sizes
s_{θ_c} = standard deviation of microcrack orientation
s_{tran} = transition value of the standard deviation of ligament sizes
D_{I}, D_{II} = equivalent dislocation density functions of modes I and II
n_{fatal} = linkage step that causes fatal collapse
$p(c)$ = ligament size distribution
P_i = further linking probability after i linkages
P^1 = probability of first coalescence dominant fracture
P^k = probability for the sustained extension of a crack after the kth linkage
R = energy ratio
w_b, w_a = deformation energy before and after the coalescence process
γ_s = surface energy
θ_a, θ_c = microcrack-orientated angles
$\sigma(x)$, $\tau(x)$ = normal and shear traction loaded on the microcrack surface
$\Delta\Pi$ = potential energy released by linking two neighbouring cracks

INTRODUCTION

Randomly distributed microcracks impose a basic damage configuration on brittle materials, which range from ceramic, concrete, to rocks. Early researches on solids weakened by microcracks were focused on the reduction of effective elastic constants. The reduction can be accurately estimated through various approaches such as the Mori–Tanaka method,[1] the self-consistent method[2] and the generalised self-consistent method.[3] Those approaches, however, are not sensitive to the local microcrack geometry and cannot serve as the fracture-related indicator of brittle materials.

Study of the fracture behaviour of brittle materials leads to research interest in macrocrack–microcrack interactions. A number of researchers[4–9] studied the interaction between a macrocrack and nearby microcracks. Hutchinson[10] and Ortiz[11,12] studied shielding by microcracks. A comprehensive review of this topic can be found in the work of Kachanov.[13] Yang *et al.*[14] and Zhang *et al.*[15] reported their recent investigation on the statistical strength of brittle materials with collinear

Correspondence: W. Yang, Department of Engineering Mechanics, Tsinghua University, Beijing, 100084, P. R. China. E-mail: yw-dem@tsinghua.edu.cn

microcracks, emphasizing the strong interactions among the microcracks.

The above research topics do not cover the macrocrack-extension process, which may dominate the fracture behaviour of the brittle materials. Recently, Zhang and Yang,[16] in exploring the extension of a macrocrack by connecting statistically distributed microcracks, discussed how long a semi-infinite crack can extend and how far the crack tip can shift vertically.

The formation of a macrocrack depends on the coalescing process of microcracks. Sketched in Fig. 1 is the general coalescing process via step-by-step microcrack linkages. A single chain of coalesced microcracks dominates the process. In this paper, a model based on the coalescence process for planar orientated microcracks will be presented.

Two typical loading patterns—displacement loading and stress loading—lead to various responses. Microcrack coalescence under displacement loading is inevitably influenced by stress relaxation in each linkage step. As a result, global softening assisted by microcracks plays an important role in the analysis.[17]

Whereas under stress loading, the elastic analysis of microcracks can be divided into two problems: the matrix without microcracks under remote stress loading and the microcracked matrix with the negating crack surface tractions. The latter dictates the coalescing process of microcracks, and is determinable in each microcrack linkage, regardless of the global softening in the coalescing process. Under this restriction, the critical linkage analysis of coalescing microcracks will be presented in this paper.

Formulation

A two-microcrack configuration representative of a coalescing step will be examined in this section. In order to analyse the coalescence of two neighbouring microcracks, an energy ratio R is introduced, which is the energetic measure of the microcrack-propagation driving force.

Representative configuration

The work assumes a self-similar coalescing process of microcracks, although their mutual orientation changes appropriately in the specific coalescing step. The assumption has two implications: (i) aside from the linking pair, other microcracks have no influence on the linkage process and (ii) the connected microcrack, through zigzag, is treated as a flat-extended crack. The first implication is somewhat justified under stress loading because the degradation of the material stiffness owing to the presence of the other microcracks does not affect the stress intensity along the connected pair. The second implication may cause local errors at the crack tips because a zigzag crack may tilt differently from a straight crack. The effect of this local distortion may become small if one considers the energy released during the whole connecting process. A representative configuration consists of the linkage of two neighbouring microcracks, as shown in Fig. 2. Attention is focused on the simple case of equal biaxial tension in order to avoid load deflection after each linkage.

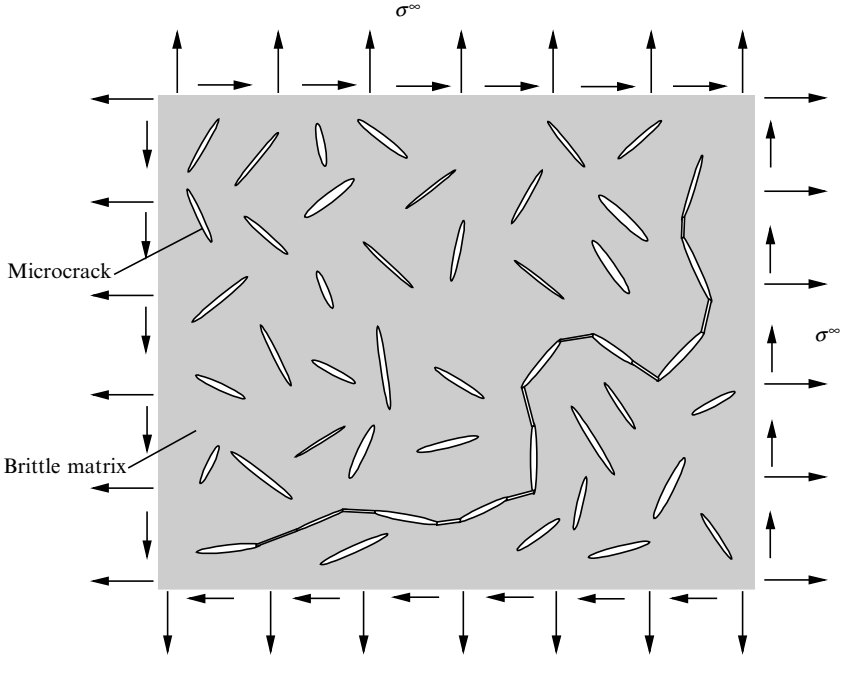

Fig. 1 Schematic of randomly distributed microcracks and a coalescence path.

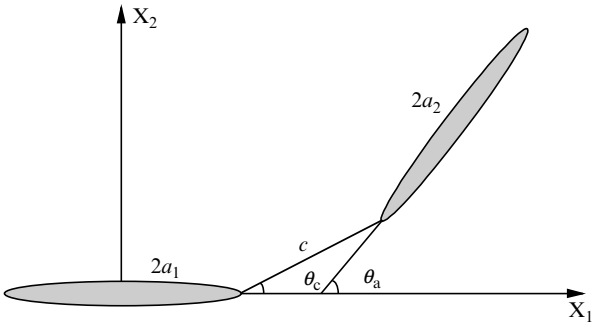

Fig. 2 Schematic of the representative configuration.

Normalised configuration parameters are:

$$\left(\frac{a_1}{a_0}, \frac{a_2}{a_0}, \frac{c}{a_0}, \theta_a, \theta_c\right)$$

where a_1 and a_2 are the half-lengths of microcracks 1 and 2; c is the ligament size; θ_c is the angle between microcrack 2 and the ligament; θ_a is the orientation difference of two microcracks. All lengths are normalised by $a_0 = \int_0^\infty af(a)\mathrm{d}a$, the expected half-length of the randomly distributed microcracks, with $f(a)$ being the density function of crack half-length.

The cracks can be simulated by continuous distributions of dislocations.[18,19] A similar formalism is adopted here in order to evaluate the elasticity field perturbed by two microcracks, with details given elsewhere.[20] The dislocation densities are given by $D(x) = D_{\mathrm{I}}(x) + iD_{\mathrm{II}}(x)$, where the subscripts I, II label the deformation modes. One can expand the density function in terms of Chebyshev polynomials of the first kind.[21] The stress and strain distributions can be expressed by the Chebyshev coefficients to be solved. The solution accuracy can be guaranteed by taking enough terms in the Chebyshev polynomials.

Energy ratio

The coalescence of the microcracks is dictated by an energy ratio defined as:

$$R = \frac{\Delta\Pi}{2c\gamma_s} \tag{1}$$

where $\Delta\Pi$ denotes the release of potential energy because of the linkage of two neighbouring cracks and γ_s is the surface tension of the brittle matrix. Accordingly, R represents the ratio between the released potential energy and the energy to create two surfaces along the broken ligament during the coalescence. The larger the ratio R, the larger the driving force, and the larger the coalescence probability. With this understanding, one defines the fracture process as a sequence of coalescing steps selected by R values. We remark that under all-around traction loading and plane strain deformation, Poisson's ratio will not have effect on the energy ratio R.

We denote $\sigma(x)$ and $\tau(x)$ as the normal and shear 'pseudotractions'[5] transferred to the microcrack surface, whose opening and sliding displacements can be calculated by the scheme outlined in the preceding section, as well as the references listed therein. The potential energy contributed from the ith microcrack is given by:

$$\Pi^{(i)} = \int_{-a_i}^{a_i} \left[\sigma(x)u_y(x) + \tau(x)u_x(x)\right]\mathrm{d}x \quad \mathrm{i} = 1, 2 \tag{2}$$

Summing over $\Pi^{(i)}$ before and after the microcrack linkage, one obtains the potential energy release $\Delta\Pi$, from which the energy ratio R follows from (1). Such a conclusion has been reached from the recent numerical calculations and analyses.

RESULTS

In this section, we evaluate the energy ratio R for two special cases: collinear and wavy microcrack configurations.

Collinear microcracks

Collinear microcracks impose the most critical configuration under a prescribed microcrack density. Without loss of generality, one may fix the half-length of one microcrack, and consider the variation of R under various lengths of the second crack and the ligament. Figure 3 shows the R surfaces as functions of a_2 and c for fixed values of a_1 of 1.0, 2.0, 3.0, 4.0 and 5.0. Grid lines on each surface correspond to curves of fixed values of a_2 or c. They indicate that R increases as a_2 increases or as c decreases. The value of R ascends rapidly near the end of small c. For a given combination of a_1 and a_2, each R–c curve has a minimum at c^* (as shown in Fig. 4a). When $0 < c < c^*$, R increases as c decreases, and rises toward infinity as c tends to zero; when $c > c^*$, R increases slowly as c increases, and approximately approaches a linear relation for large c. Figure 4(b) depicts the R–c curves for small ligament size where microcrack coalescence is likely to occur. They will serve as the basic curves for the subsequent analysis.

Wavy microcracks

A wavy microcrack array is a representative configuration for coalescing microcracks. We will illustrate the variations of R under various combinations of microcrack

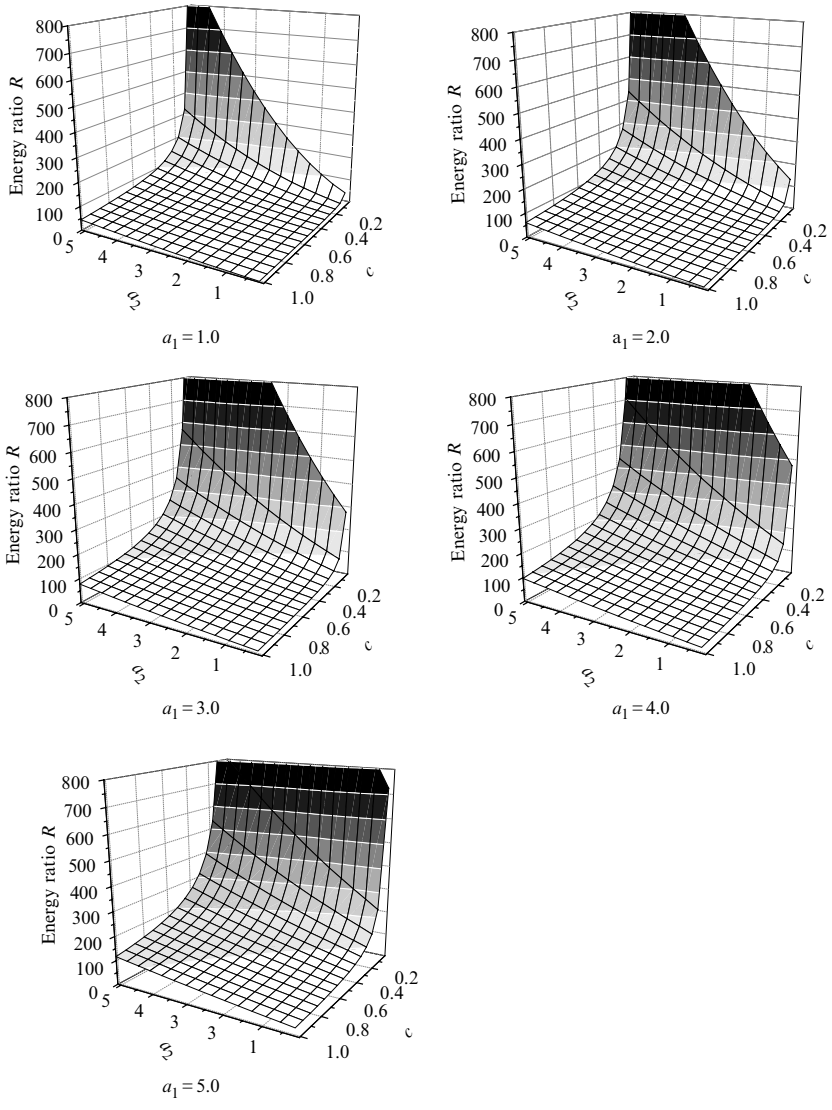

Fig. 3 $R-(a_2,\ c)$ surfaces under various a_1 values.

lengths, ligament sizes and orientations in this case hereafter.

Figure 5a–d shows the contours of the $R-(\theta_a,\ \theta_c)$ surface for equal microcrack length a_0, but various ligament sizes, where $a_0 = 1.0$ and $c = 0.1,\ 0.5,\ 1.0,\ 1.5$, respectively. All contours depict the decreasing trend of R with the increase of θ_a or θ_c. The R value always maximises at $\theta_a = 0$ and $\theta_a = 0$, namely the collinear configuration. For a given θ_c (or θ_a), the R –θ_c (or θ_a) curve reaches its peak at a certain θ_c (or θ_a) value which has the same sign as θ_a (or θ_c). The larger the value of θ_a (or θ_c), the larger the peak location θ_c (or θ_a). This trend becomes pronounced in the case of larger c–a values. Comparing the four maps, one finds that a larger a–c value indicates a larger overall R level, thus a stronger interaction, which is consistent with the collinear configuration.

Figure 6 a–c shows the contour maps of the $R-(\theta_a,\theta_c)$ surface when $a = 1$ and $c = 0.5$. Various maps correspond to various coalescing stages: map (a) denotes the initial configuration without any microcrack linkages; map (b) the configuration after the first linkage and map (c) the configuration after the second linkage. Tracking the variations of R with the coalescing steps, one finds that even the minimum R value in a certain step exceeds the maximum R value of the previous steps. For the case of equal microcrack length and ligament size, the microcracks connected by the first linkage will dominate and lead to the fatal collapse.

Figure 7a–d shows the R surfaces with respect to c and θ_c for fixed value of $\theta_a = 0$ and $a = 1.0$. Various surfaces correspond to various coalescing stages, in the same sense as explained before. Grid lines on each surface correspond to curves for fixed values of c or θ_c. These surfaces indicate that R increases as c decreases and rises toward infinity when c tends to zero. On the other hand, R decreases as the absolute value of θ_c increases and

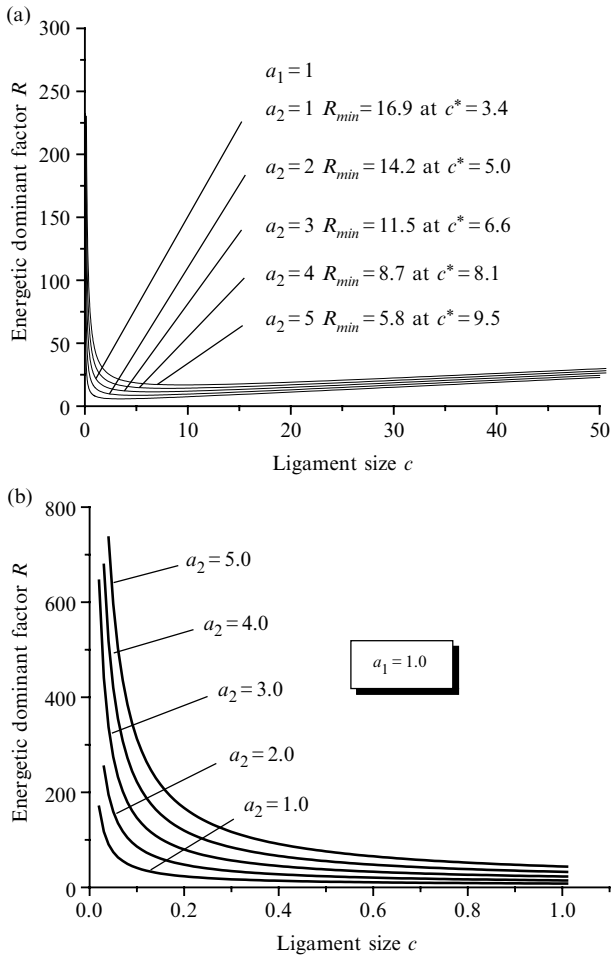

Fig. 4 $R - c$ curves: (a) for large c range; (b) local zoom-out for small c.

always reaches its maximum at $\theta_c = 0$, which renders the $R - (c,\theta_c)$ surface a shape of a half-saddle. Comparing various coalescing stages, one finds that the R level increases as the crack extends step by step. These graphs will be exploited in the next section for the critical linkage-dominated fracture analysis.

DISCUSSION

In this section, we carry out the probability analysis of the critical linkage-dominated fracture. Variations of the probability vs. microcrack geometry and statistics are calculated for the two cases of collinear and wavy microcracks. The critical linkage steps are identified under various ligament sizes and microcrack-orientation distributions.

Collinear microcrack configuration

Recall that microcrack coalescence occurs under strong interaction. Accordingly, the small ligament size range, say $c < c^*$, is of interest to us. In that range, R increases as c decreases (as shown in Fig. 4b).

Consider the case where all microcracks have the same half-length of $a_0 = 1.0$ and are separated by ligaments whose sizes are described by a normal distribution $p(c)$. For successive linking steps, the variations of R with respect to ligament size c can be seen in the various curves in Fig. 8. The top graph plots energy ratios for the initial configuration ($R_0(c)$ curve), after the first linkage ($R_1(c)$ curve) and after the second linkage ($R_2(c)$ curve), and so

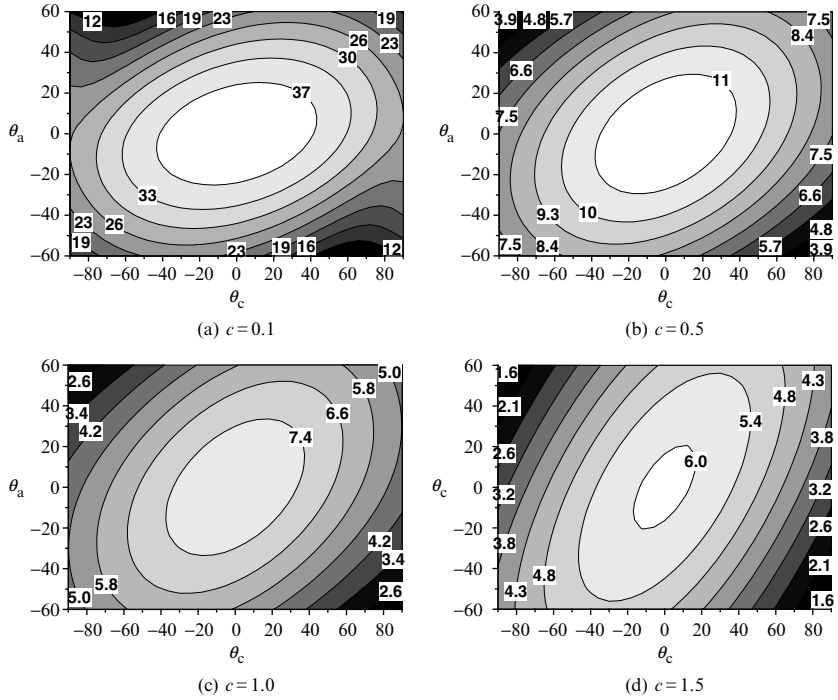

Fig. 5 Contours of $R - (\theta_a, \theta_c)$ surface with $a_0 = 1.0$.

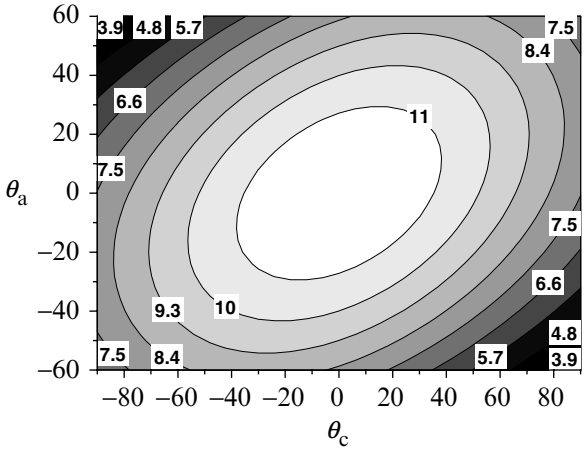

(a) Initial configuration

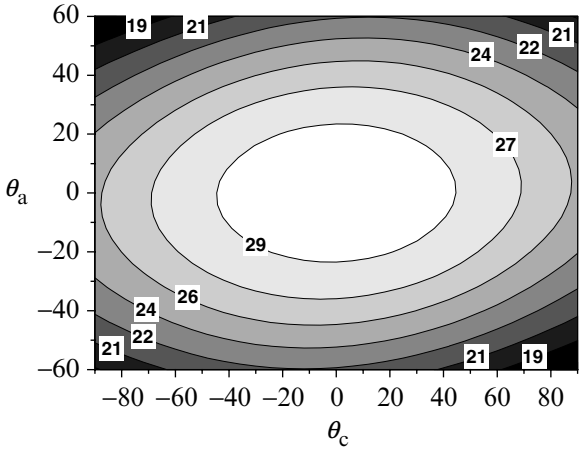

(b) After the first linkage

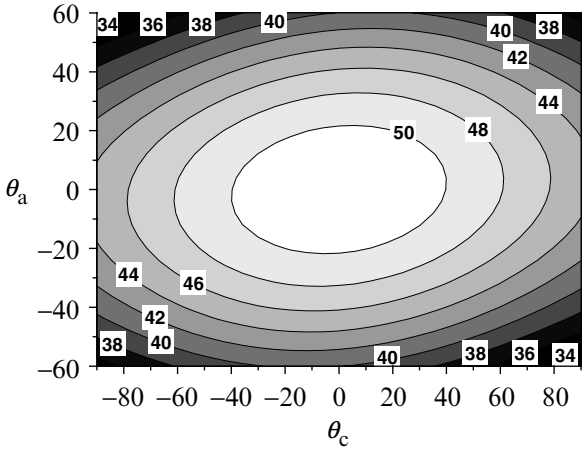

(c) After the second linkage

Fig. 6 Contours of $R-(\theta_a,\ \theta_c)$ surface.

on. Those curves are based on a linkage calculation between an initial microcrack of length $2a_0$ and a connected crack of length $(2i+2)a_0+ic_0$, separated by a ligament of c. The bottom graph depicts $p(c)$ that assumes a normal distribution with an expected value of c_0.

For a given ligament size c, one can find an energy ratio $R_i(c)$ for a crack that has connected i times. Dictated by the same energy ratio, a critical ligament size $c_i = R^{-1}{}_0(R_i(c))$ can be defined, as graphically depicted in Fig. 8. For two neighbouring microcracks of initial half-length a_0, linkage between them is impossible if their ligament is larger than c_i. Consider all possible ligament size c; the proportion of ligaments whose sizes are larger than c_i is

$$\int_{c_i(c)}^{\infty} p(c')\mathrm{d}c'$$

as indicated by the shaded area in the bottom graph of Fig. 8. By the random encounter of ligament size of the connected crack, the value of

$$\int_{c_i(c)}^{\infty} p(c')\mathrm{d}c'$$

also gives the probability of the connected crack (after i linkages) for further extension across a ligament of size c, under the same driving force related to $R_i(c)$. The integration of that quantity with respect to c, weighted by the normalised density $p(c)$, delivers the further linkage probability for a crack that has connected i time:

$$P_i = \int_0^{\infty} p(c) \int_{c_{i(c)}}^{\infty} p(c')\mathrm{d}c'\mathrm{d}c \tag{3}$$

For a connected crack after the kth linkage, the probability for that crack to reach a fatal state (under the same driving load) is calculated by the multiplication of further linkage probability P_i as:

$$P^k = \prod_{i=k}^{n_{\mathrm{fatal}}} P_i \tag{4}$$

where n_{fatal} denotes the number of linkages to form a fatal crack, determined by the remote loading and the matrix fracture toughness.

The concept of the critical linkage in statistically coalescing microcracks now emerges. The coalescence of microcracks is said to be dominated by one connected crack if its sustained extension, rather than the linkage of other microcracks, leads to the formation of a fatal crack. Accordingly, the difference:

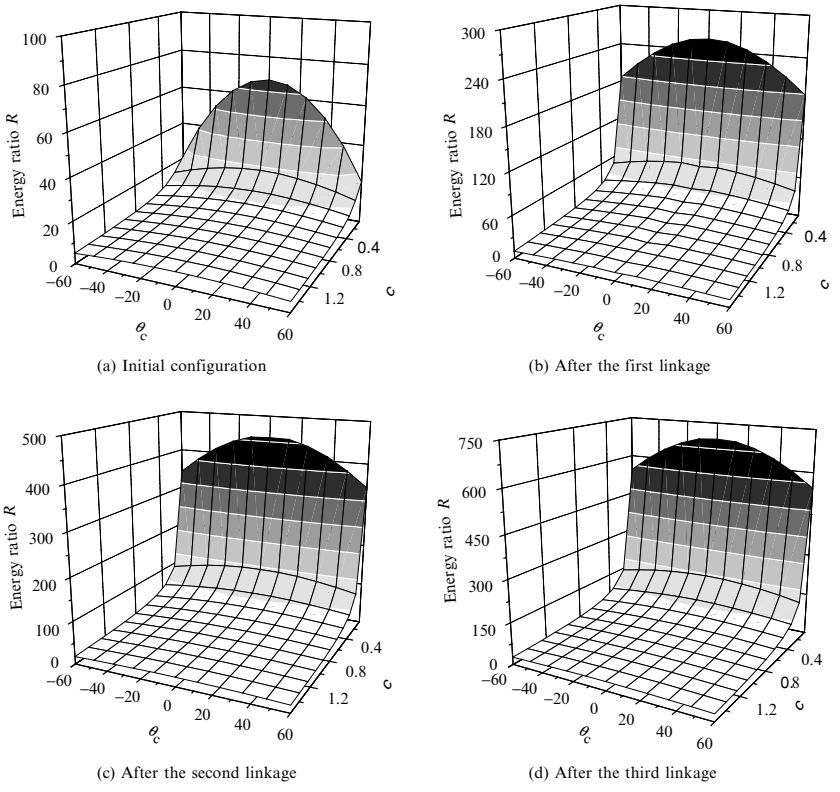

Fig. 7 $R-(c,\ \theta_c)$ surfaces of various linkage steps.

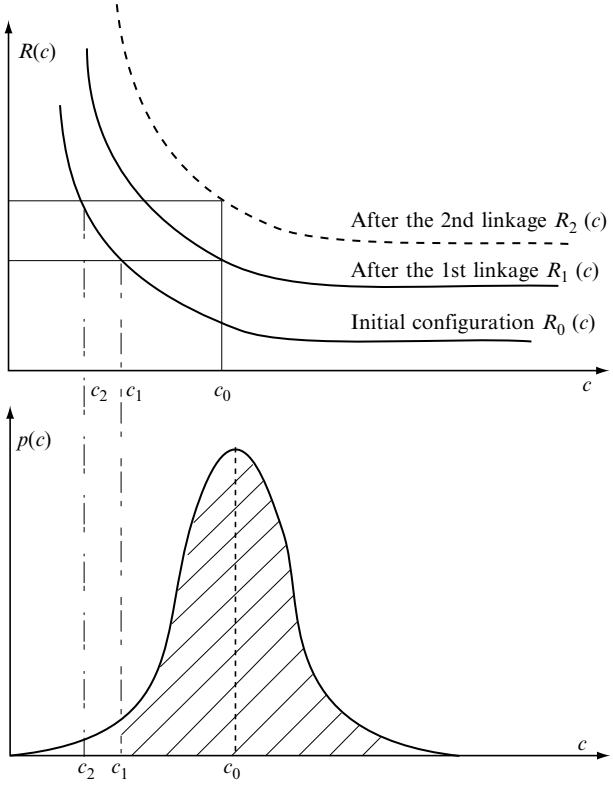

Fig. 8 Critical linkage in coalescing microcracks. Top graph shows *R–c* curves of various; linkages bottom graph depicts probability distribution of ligament size *c*.

$$\Delta P^k = P^k - P^{k-1}, \quad P^0 = 0 \tag{5}$$

denotes the probability of crack coalescence dominated by the *k*th linkage. Specifically, the probability of microcrack coalescence dominated by the first linkage is denoted by P^1.

Given a certain microcrack distribution and geometrical parameters, one can determine the probability of microcrack coalescence dominated by the first linkage. Figure 9 plots the variation of P^1 under various expected ligament sizes c_0 and standard deviations s. The curves are calculated under $a_0 = 1.0$ and $c_0 = 0.3,\ 0.5,\ 0.8$. The plots illustrate the fact that the probability P^1 decreases as s increases. The case of $s = 0$ corresponds to periodic microcracks and is always dominated by the first linkage. A transition value s_{tran} of the standard deviation of ligament sizes can be defined. When $s < s_{\text{tran}}$, microcrack coalescence is dominated by the first linkage; otherwise, it is dominated by subsequent linkages. As the expected ligament size increases, the transition value s_{tran} increases and the transition becomes smoother.

Figure 10 shows the probability of microcrack coalescence dominated by the first linkage and the subsequent linkages. It plots the variations of P^k ($k = 1,\ 3,\ 5,\ 8,\ 10$) with respect to the standard deviations, with $a_0 = 1.0$,

$c_0 = 0.8$. The horizontal line of $P^{n\text{fatal}}(s) = 1$ gives the correct upper limit of that family of curves. The vertical distance between the two curves (say between the curve of $k = 3$ and the curve of $k = 5$) denotes the probability of microcrack coalescence dominated by the linking steps in the designated k range (say for $k = 4$ and 5). The higher the value of the standard deviation of the crack ligaments, the larger the critical linkage that would dominate the microcrack coalescence.

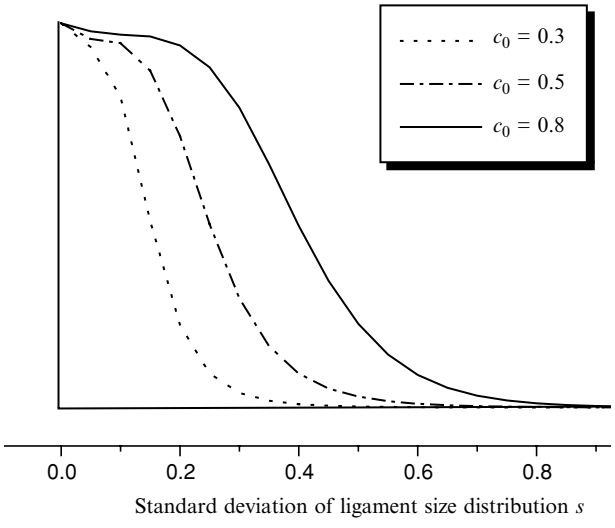

Fig. 9 Probability of microcrack coalescence dominated by the first linkage.

Wavy microcrack configuration

The relationship between coalescing types and geometry of wavy microcrack configuration is discussed next. Our analysis is based on Fig. 7, in which $a_0 = 1.0$ and $\theta_a = 0$. The distributions of c and θ_c are denoted by $p_c(c)$ and $p_\theta(\theta_c)$, respectively. For a given combination of ligament size c and orientated angle θ_c, one can find an energy ratio $R_i(c,\theta_c)$ for a crack that has connected i times. With the same energy ratio, the corresponding area A_i in the c–θ_c plane can be identified in the initial configuration (Fig. 7a) where $R_0(c,\theta_c) < R_i(c,\theta_c)$. Considering all possible ligament sizes c and orientation angle θ_c, one derives the probability for further extension of a crack that has already connected i times as:

$$P_i = \int_{-\theta_c^{\max}}^{\theta_c^{\max}} \int_0^\infty p_c(c) p_\theta(\theta_c) \left[\iint_{A_i} p_c(c') p_\theta(\theta_c') \, dc' d\theta_c' \right] dc d\theta_c \tag{6}$$

where $\theta_c^{\max}$ denotes the maximum orientated angle. After the kth linkage, the probability for sustained extension of that crack is also given by (4).

Figure 11 plots the fracture probability dominated by the first linkage under various ligament size distributions, and gives a comparison of P variations along various microcrack-orientation distributions. Curves in Fig. 11 are calculated for $a_0 = 1.0$, $c_0 = 0.5$, $\theta_a = 0.0$, and θ_c is described by a normal distribution with expected value of zero and standard deviation of s_{θ_c}. Various curves in Fig. 11(a) correspond to various s_{θ_c} of 0° (collinear distribution), 5°, 10 and ∞ (even orientation distribution). The plots depict the same decreasing

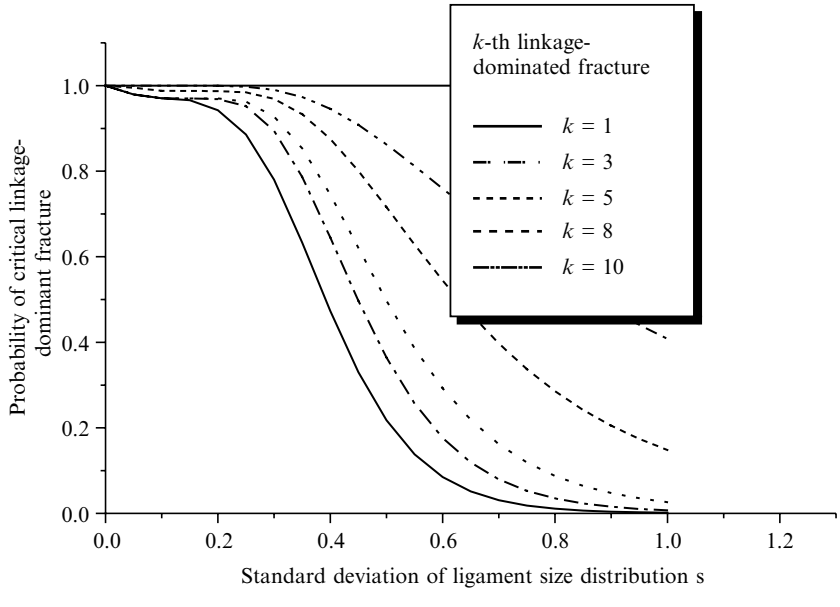

Fig. 10 Probability of microcrack coalescence dominated by the first linkage and subsequent linkages.

trend of P as s increases. For a given microcrack half-length and ligament size distribution, the probability of first linkage-dominated fracture increases as the microcrack-orientation randomness increases. Also, the wavy microcrack configuration exhibits a greater chance of the fracture mode being dominated by the first linkage than the collinear one. This can be explained by the fact that the ligament between two unconnected microcracks in the collinear configuration is more likely to be broken in the further linkage steps than the one in the wavy configuration.

Figure 11b plots P–s curves under various expected ligament sizes of $c_0 = 0.3, 0.5, 0.8$. The dashed line and solid line denote the collinear and wavy (symmetric orientation distribution) microcrack configuration, respectively. The wavy case has a relatively higher P level and a milder transition than those for the collinear case. The transition value s_{tran} defined in Fig. 9 also increases as c_0 increases.

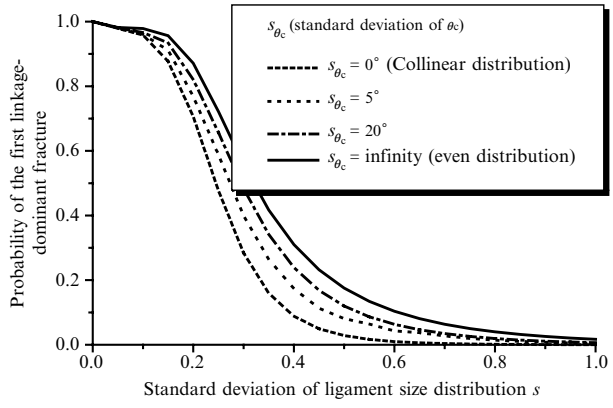

(a) P–s curves under microcrack various-orientation distribution

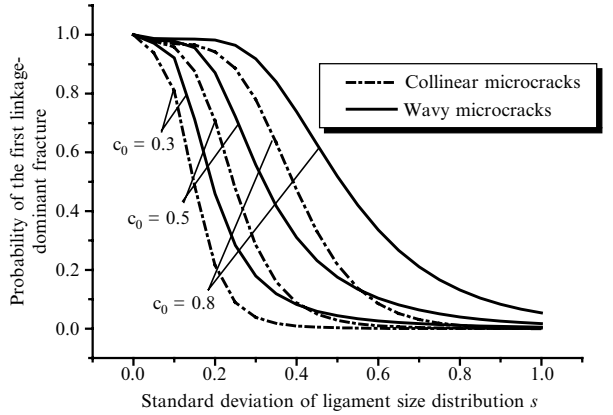

(b) P–s curves under various expected ligament size

Fig. 11 Probability of microcrack coalescence dominated by the first linkage.

Figure 12 plots the probability of microcrack coalescence dominated by the first linkage and the subsequent linkages. The curves are calculated for a wavy microcrack configuration of $a_0 = 1.0$, $c_0 = 0.8$ and critical linkage step numbers of 1, 3, 5 and 8. The probability level increases as the critical linkage number increases, similarly to the trend shown in Fig. 10. Comparison between the two corresponding curves with the same critical linkage number in Figs 10 and 12 shows the relatively higher P level of the wavy microcrack configuration than the collinear one, and the P level difference becomes larger as the critical linkage number increases. For example, the computational result of the 8th linkage-dominated fracture probability in wavy configuration is a horizontal line. This means that, for the wavy microcrack distribution of $a_0 = 1.0$, $c_0 = 0.8$ and $\theta_a = 0.0$, the 8th microcrack linkage will inevitably lead to a fatal collapse, no matter what ligament size randomness the microcracks possess.

CONCLUSION

The fracture process of brittle materials with randomly orientated microcracks critically depends on strong interactions among microcracks and the coalescence path leading to a fatal crack. The coalescence of microcracks is controlled by the energy ratio R between the release of potential energy and the energy to create the new crack surface. The influences on R of various geometrical and statistical parameters have been calculated for collinear and wavy microcrack configurations.

The present work studies the critical linkage-dominated fracture based on the energy ratio. For a wavy array consisting of microcracks of equal length and ligament size, microcrack coalescence is dominated by the first linkage, regardless of the random orientations of the microcracks. For both the collinear and wavy microcrack configurations, the critical linkage-dominated fracture becomes less probable as the standard deviation of ligament size increases. The wavy microcrack configuration displays a greater chance of the fracture mode being dominated by the given critical linkage number than the collinear one. The probability difference between the two configurations becomes larger and larger as the number of critical linkage increases. These quantitative relations may guide the optimal design of material mesostructure. Further investigations are required in order to explore the quantitative relationship between the critical linkage-dominated fracture and the strength and toughness of microcrack-weakened brittle solids, as well as the shielding of neighbouring microcracks to the coalescing chain. For microcrack coalescence under displacement loading, global softening is involved. In this case, the analysis would rather focus on the expected

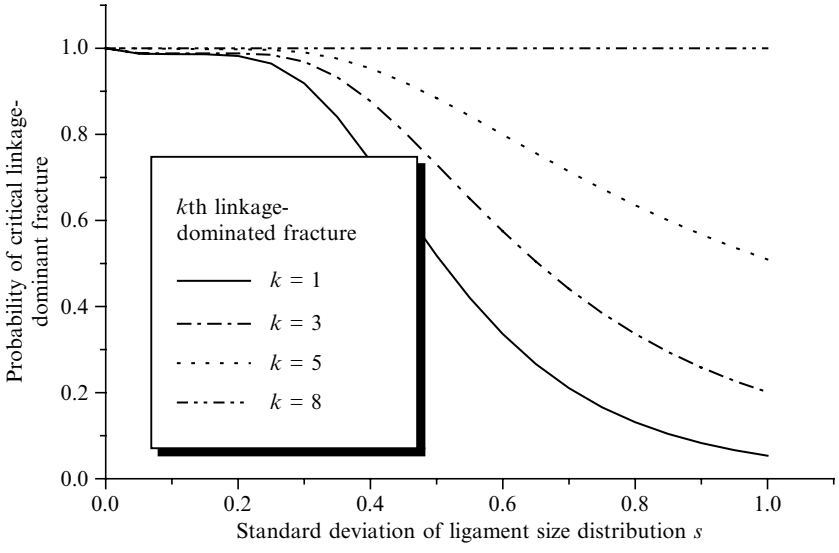

Fig. 12 Probability of microcrack coalescence dominated by the first linkage and subsequent linkages.

length of the coalescing microcracks, as is discussed by Li and Yang.[17] Another issue of importance is to design experiments that can identify the statistical characteristics of the critical linkage.

REFERENCES

1 Mori, T. and Tanaka, K. (1973) Average stress in matrix and average elastic energy of materials with misfitting inclusions. *Acta Metall.* **21**, 571–583.
2 Budiansky, B. and O'Connell, R. J. (1976) Elastic moduli of a cracked solid. *Int. J. Solids Struct.* **12**, 81–97.
3 Christensen, R. M. and Lo, K. H. (1979) Solutions for effective shear properties in three phase sphere and cylinder models. *J. Mech. Phys. Solids* **27**, 315–330.
4 Rubinstein, A. A. (1986) Macrocrack–Microdefect Interaction. *ASME J. App. Mech.* **53**, 505–510.
5 Kachanov, M. (1987) Elastic solids with many cracks: a simple method of analysis. *Int. J. Solids Struct.* **23**, 23–43.
6 Horii, H. and Nemat-Nasser, S. (1987) Interacting Micro-Crack Near the Tips in the Process Zone of a Macro-Crack. *J. Mech. Phys. Solids* **35**, 601–629.
7 Chudonovsky, A., Dolgopolsky, A. and Kachanov, M. (1987) Elastic interaction of a crack with a microcrack array 3/4Part I and Part II. International. *J. Solids Struct.* **23**, 1–21.
8 Gong, S. X. and Horii, H. (1989) General solution to the problem of microcarcks near the tip of a main crack. *J. Mech. Phys. Solids* **37**, 27–46.
9 Kachanov, M., Montagut, E. and Laures, J. P. (1990) Mechanics of crack–microcrack interactions. *Mech. Mater.* **10**, 59–71.
10 Hutchinson, J. W. (1987) Crack tip shielding by microcracking in brittle solids. *Acta Metall.* **35**, 1605–1619.
11 Ortiz, M. (1987) A continuum theory of crack shielding in ceramics. *ASME J. App. Mech.* **54**, 54–58.
12 Ortiz, M. (1989) Maximal crack-tip shielding by microcracking. *ASME J. App. Mech.* **56**, 279–283.
13 Kachanov, M. (1992) Effective elastic properties of cracked solids: critical review of some basic concepts. *App. Mech. Rev.* **45**, 304–335.
14 Yang, W., Zhang, S.-T. and Li T.(1997) Strong interaction among randomly distributed microcracks. *Proceedings of the Ninth International Conference on Fracture* **4**, 1971–1978.
15 Zhang, S.-T., Li, T. and Yang, W. (1998) Statistical strength of brittle materials with strongly interacted collinear microcracks. International. *J. Solids Struct.* **35**, 995–1008.
16 Zhang, S.-T. and Yang, W. (1998) Macrocrack extension by connecting statistically distributed microcracks. *Int. J. Fract.* **90**, 341–353.
17 Li, T. and Yang, W. (2001) Expected coalescing length of displacement loading collinear microcracks. *Theoret. Appl. Fracture Mechanics.* **36**, 17–21.
18 Han, X. and Wang, T. (1996) A general method for solving the problem of both open and closed multiple cracks. *Int. J. Fract.* **76**, 69–72.
19 Freij-Ayoub, R., Dyskin, A. V. and Galybin, A. N. (1997) The dislocation approximation for calculating crack interaction. International. *J. Fract.* **86**, L57–L62.
20 Li, T. (2000) Coalescence of Microcracks in Brittle Materials. PhD Thesis, Department of Engineering Mechanics, Tsinghua University, Beijing, China, 6–29.
21 Erdogan, F. (1997) Complex function technique. In: *Continuum Physics*, Vol. II, pp. 523–603. Academic Press, New York.